- Technical Paper -

CHARACTERIZATION OF MICROCRACKING IN VERY EARLY AGE CONCRETE SUBJECTED TO ELEVATED TEMPERATURE BY AE

Ha Ngoc SON[*1], Akira HOSODA[*2], Takeshi WATANABE[*3]

ABSTRACT

AE technique was used to characterize microcracking in concrete from the age of 1.5hrs, under temperature from 20 to 60°C. Microcracks occurred considerably in the cooling period. Driving force induced by incompatibility of deformation between mortar and coarse aggregate. The tendency of tensile strength loss agreed with AE results. Damage in GGBFS concrete was severer than that in OPC concrete due to larger number of small microcracks. Concrete was deteriorated considerably under cyclic temperature. Mitigating measures by using LWA and coarse aggregate of suitable type and size were proposed.

Keywords: Microcracking, acoustic emission, early age concrete, elevated temperature, blast furnace slag

1. INTRODUCTION

Concreting in hot weather, heat curing, mass concrete are typical cases where temperature in concrete is raised significantly at very early ages. The subsequent stage is a cooling period. This variation of temperature apparently makes concrete deformed. In addition, autogenous shrinkage is also developed quickly in this period. These deformations are principles inducing stresses in concrete even in case no external force is applied, no external restraint and no temperature gradient within structure exist. Intensive localized stress is expected in mortar around coarse aggregate. This stress is resulted by the incompatibility in deformation between mortar and coarse aggregate. When the stress in mortar exceeds its strength, microcracking will take place.

Acoustic emission (AE) technique appears to be advanced in tracking the deterioration with a wide range from microscale to macroscale. Its sensitivity is high enough to listen to a microcracking in material. When a set of AE signals is recorded, it is possible to analyze various parameters to understand the mechanism and process of the deterioration. In this research, AE technique was selected to study the characteristics of deterioration of concrete from a very early age under elevated temperature condition.

2. EXPERIMENTAL PROGRAM

AE tests were conducted on concrete specimens from a very early age with the variation of temperature. The specimens were subjected to no external restraint or external load. Microcracks were generated by local stress in mortar under the restraint of coarse aggregate against the deformation of mortar. This restraint was the result of the incompatibility in deformations of the two components of concrete: mortar and coarse aggregate.

2.1 Acoustic emission

AE is defined as elastic waves produced by microfracturing in a solid [1], and is related to an irreversible release of energy. AE technique allows detection of elastic waves emitted by microcracking inside concrete.

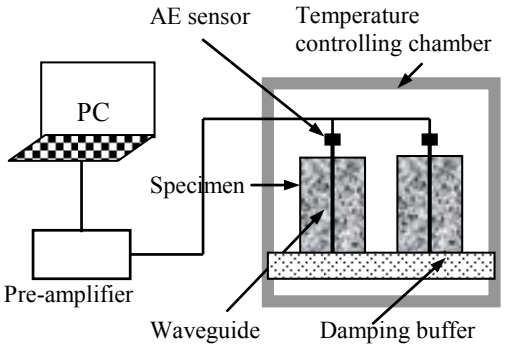

Fig. 1 AE test system

Fig. 1 describes the experimental system for AE tests. Two-channel AE system was used. Sensors were 150 kHz resonant type, the type for general purpose with operating temperature of -65°C to 177°C. The AE sensors were coupled with stainless steel wave-guides which were embedded in concrete specimens. All specimens, wave-guides and AE sensors were placed in a temperature controlling chamber. In each test, two AE sensors were used for two separate specimens cast from the same mix batch. Then, the average was taken for the measured values.

Noise is always the persisting problem of AE test.

*1 PhD student, Grad. School of Envir. & Infor. Sciences, Yokohama National University, JCI Member
*2 Associate Prof., Grad. School of Envir. & Infor. Sciences, Yokohama National University, Dr.E, JCI Member
*3 Assistant Prof., Dept. of Civil & Envir. Engineering, The University of Tokushima, Dr.E, JCI Member

Curing concrete specimens inside the temperature controlling machine makes AE test need special cares to deal with significant noises and vibration generated by the dynamic parts of the machine. Trial tests had been conducted to make the practical elimination of noises possible. A damping buffer was used to discard vibration and separating noises from the machine transmitted by contacting metal parts to the specimens. The electric pulses and sound waves sent from outside sources through air were rejected by setting threshold level of 40 decibel (dB). The sensitivity of the AE sensors used in this research was checked by fully calibrated sensors.

Since acoustic wave was measured from as early as one and half hour from the mixing time when concrete is still in plastic form, the AE sensors could not be directly coupled to the specimens. To solve this problem, AE wave-guides were employed (Fig. 2). The wave-guide consists of a stainless steel rod with 4mm in diameter, which will be embedded in the specimen, and a sensor seat on the top. A rubber tight was used to slightly attach the sensor to the wave-guide. Silicon based grease couplant was used. As the attenuation of AE wave in steel is one order of magnitude smaller than that in concrete [2], the wave amplitude loss while transmitting in the waveguide can be neglected.

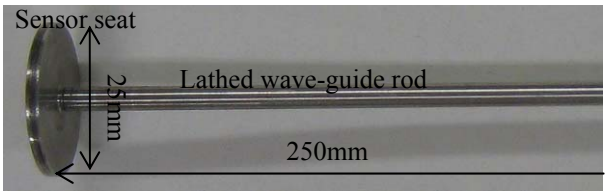

Fig. 2 AE wave-guide

Cylindrical steel moulds were used for all AE tests (Fig. 3a). A layer of 0.5mm thick teflon sheet was placed covering the whole inside face of the mould. All specimens were sealed with polyethylene film. The height of concrete specimens was 200mm and that of mortar was 133mm. This difference was due to coarse aggregates were removed from the same volume of concrete mix to make the mortar specimen.

2.2 Measurement of deformation

Fig. 3b describes the method for the measurement of total deformation of a specimen using an embedded strain gauge. The strain gauge was PMFL-60-2LT type, 60mm in length and 4mm in diameter. The design of I shaped strain gauge improves the mechanical link with concrete. The preparation of specimens was same as that for the AE test. Two specimens of the same mix batch were tested at the same time and the average of the two was taken.

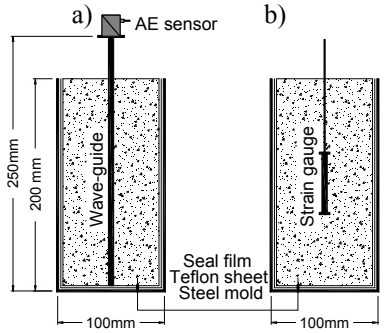

Fig. 3 Specimen preparation for (a) AE test; and (b) deformation test

2.3 Measurement of CTE

Coefficients of thermal expansion (CTE) of mortars and aggregates were measured. Tests of CTE for mortar were conducted at the age of one day after being subjected to heat curing. The method was same as that for the deformation test. Specimens were heated from 20°C to 50°C in two hours then kept at 50°C for 2 hours before being cooled down to the original level. CTE was calculated separately for heating and cooling periods. After that the average of these two values was derived. This method allowed separation of autogenous shrinkage from the CTE measuring results because autogenous shrinkages developed in heating and cooling periods would cancel each other in the average. The measurement method for CTE of coarse aggregates can be found elsewhere [3].

2.4 Materials

Table 1 shows the chemical composition of cementitious materials used in the current research, including ordinary Portland cement (OPC) and ground granulated blast furnace slag (GGBFS).

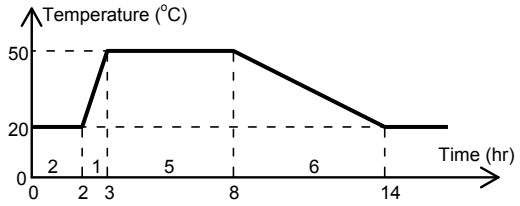

Fig. 4 Curing temperature

Two types of coarse aggregate used in this experimental program were crushed limestone and crushed andesite. The implication of this selection was the significant difference in CTE of these two rocks. Natural pit-sand and light weight aggregate (LWA) with maximum particle size of 4.75mm were the two types of fine aggregate. LWA with specific weight in completely dry condition of 1.72 g/cm^3 and water absorption of 13.4% in weight was used. A method for calculation of internal curing water using LWA can be found in the proposal of Bentz et al. [4].

Table 1 Chemical composition of cementitious materials

Type	Chemical composition										Density (g/cm^3)	Spe. area (cm^2/g)
	SiO_2	Al_2O_3	Fe_2O_3	CaO	MgO	SO_3	TiO_2	MnO	Na_2O	K_2O		
OPC	21.18	5.18	2.86	64.39	1.70	2.00	0.27	0.08	0.25	0.56	3.15	3390
GGBFS	33.29	13.68	0.29	42.73	5.10	1.9	0.55	0.33	0.20	0.31	2.89	4320

Table 2 Mixture proportion

Mix (1 m^3)	water (kg)	OPC (kg)	GGBFS (kg)	pit-sand (kg)	LWA (kg)	coarse agg. (kg)	Super-plas. (kg)	W/B ratio
M-O-30	256	853	-	1214	-	-	3.4	0.3
M-S-30	256	427	427	1158	-	-	3.4	0.3
M-S-LWA-30	256 (84)	427	427	384	613	-	4.3	0.3
C-O-L20-30	170	567	-	806	-	836** (L)	4.0	0.3
C-S-L10-30	170	283	283	796	-	825* (L)	3.7	0.3
C-S-L20-30	170	283	283	796	-	825** (L)	4.0	0.3
C-S-L20-LWA-30	170 (56)	283	283	255	407	825** (L)	4.3	0.3
C-S-A10-30	170	283	283	796	-	783* (A)	3.7	0.3
C-S-A20-30	170	283	283	796	-	783** (A)	4.0	0.3
C-S-A40-30	170	283	283	796	-	783*** (A)	4.3	0.3
C-O-L20-50	170	340	-	900	-	933** (L)	0.0	0.5
C-S-L20-50	170	170	170	893	-	926** (L)	0.0	0.5

(56) Internal curing water; (L): limestone; (A): andesite; * Dmax=9.5mm; ** Dmax=19mm; *** Dmax=37.5mm

Mix proportions for mortar and concrete are presented in Table 2. Time for preparing specimens including installing strain gauges, wave-guides and sensors was around 30 minutes. Right after that, all specimens were sealed and placed in the temperature controlling chamber which had been maintained at 20°C. The heating then started, at two hours after adding mixing water to the mix, as shown in Fig. 4.

3. RESULTS AND DISCUSSION

3.1 AE hit, count and energy

Fundamental AE parameters including number of AE hits, counts and AE energy were used to clarify the differences in damage degrees in different concretes. These parameters are presented in Fig. 5.

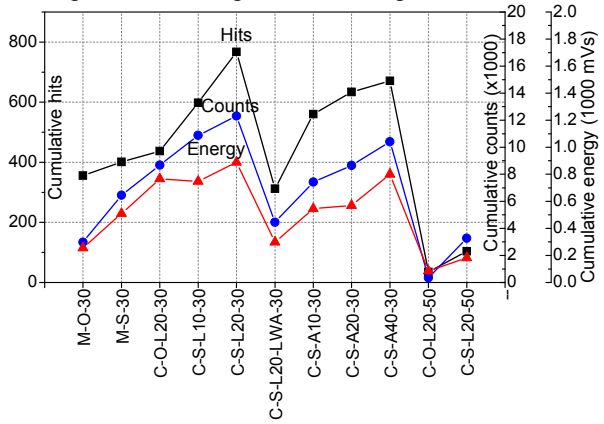

Fig. 5 Cumulative AE hits, counts and energies up to the age of 20 hours

Similar trends could be seen for hits, counts and energy among various mortars and concretes. Because the magnitude of event plays an important role in evaluation of degree of deterioration, AE energy is usually preferred over pure number of hits. It is possible to use AE energy to judge the fracture degree because AE energy and fracture energy are correlated [5].

Considering concrete with water-to-binder ratio (w/b) of 0.3, as shown in Fig. 5, the highest AE energy was registered for C-S-L20-30**.** In this mix, limestone coarse aggregate, which has the lowest CTE (Table 3), was combined with GGBFS mortar, which showed the highest net shrinkage (Fig. 6). Net shrinkage was defined elsewhere [6] as the total shrinkage considered from the peak expansion including both thermal and autogenous shrinkages. This difference led to the most unexpected incompatibility in deformation between coarse aggregate and mortar. As a result, microcracking in mortar of this concrete was probably the severest. This explained for the highest cumulative AE hits and energy measured for the C-S-L20-30 concrete. The lowest cumulative number of hits as well as energy was for concrete with LWA, C-S-L20-LWA-30. In Fig. 6, LWA mortar showed the lowest net shrinkage. This was due to almost all autogenous shrinkage was eliminated by internal curing using saturated fine LWA. Due to the smallest net shrinkage, the incompatibility in deformation between coarse aggregate and LWA mortar was also the least and probably led to the lowest magnitude of microcracking, and then in turn, the lowest cumulative AE hits and energy.

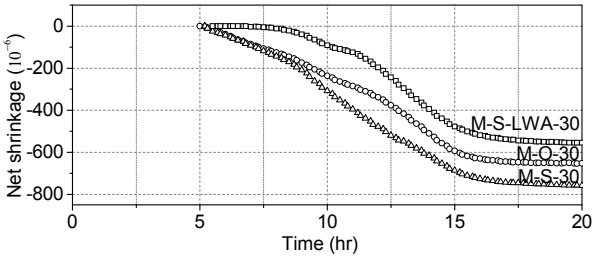

Fig. 6 Net shrinkage of mortar

Table 3 CTE of mortar and coarse aggregate

Material	*CTE (10^{-6}/°C)*
M-O-30	12.3
M-S-30	14.8
M-S-LWA-30	16.5
Limestone	6.1
Andesite	12.2

Another difference observed in Fig. 5 is related to concretes with different types of coarse aggregate. Both limestone and andesite have lower CTE than mortars (Table 3). However, limestone has far lower CTE as compared with mortars. Again, the difference in deformation between mortar and coarse aggregate was probably the origin of differences in AE parameters of concretes with limestone and andesite. Considering

concrete with coarse aggregate with Dmax of 19mm, C-S-L20-30 released AE energy of 889mVs corresponding to 767 hits detected while those for C-S-A20-30 were 570mVs and 634 hits respectively up to the age of 20 hours. The same trend was observed for concrete with coarse aggregate with Dmax of 9.5mm.

As for the effect of maximum size of coarse aggregate, it is well known that the tensile strength of concrete decrease with the increase of max size of aggregate [7, 8]. Here, it was revealed that one of the reasons for the reduction of tensile strength of concrete with larger size of coarse aggregate is the worse degree of microcracking. In both limestone and andesite concretes, accumulation of AE hits and energy increased with the increase of aggregate size (Fig. 5). This indicated the magnitude of microcracking increased with the increase of aggregate size.

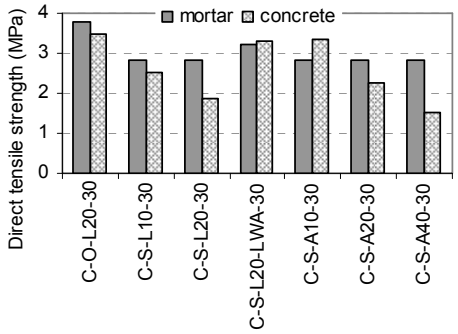

Fig. 7 Direct tensile strength of mortar and concrete

Fig. 7 compares direct tensile strengths of concretes with those of respective mortars. The losses of tensile strength of concretes as compared with those of respective mortars and cumulative AE energies at the age of 20 hours are plotted in Fig. 8. These losses are the fractions of the differences between direct tensile strength of concretes with that of respective mortars over tensile strength of mortars. In case direct tensile strength of concrete is smaller than that of mortar, the loss is a positive number and vice versa. Clearly there was a correlation between AE energy released and the loss of tensile strength of concrete. However, the data were rather scattered to build a functional relationship.

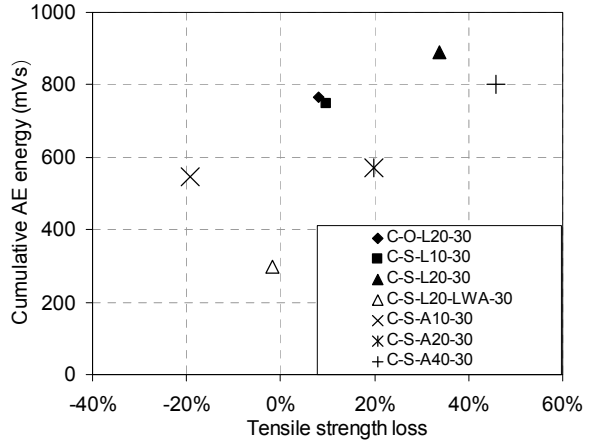

Fig. 8 Cumulative AE energy (up to 20 hours) vs tensile strength loss of concrete

For concretes with w/b of 0.5, cumulative hits, counts and energy were all significantly lower than those of concretes with w/b of 0.3. These differences might be explained by the lower net shrinkage of mortar with w/b of 0.5, due to smaller autogenous shrinkage, while thermal deformations of aggregates are independent on w/b. Another reason might be the lower stiffness of mortar with w/b of 0.5. Higher degree of attenuation of AE wave in higher moisture material might also be a cause [9].

AE energy rates, the average AE energy per hit, of concretes are plotted in Fig. 9. With the same w/b, concretes with GGBFS showed lower energy rates than concretes with OPC alone. As AE energy and fracture energy are correlated, smaller energy release of one hit may infer that cracking occurred at a lower stress. This may imply that when GGBFS mortar was combined with coarse aggregate, the concrete was more susceptible to microcracking. The weakness of GGBFS concrete could be attributed to the lower cracking resistance of GGBFS mortar at early ages.

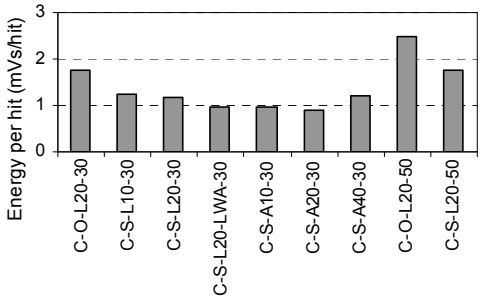

Fig. 9 AE Energy rate per hit

3.2 *b*-value

b-value is the slope of the amplitude frequency distribution of AE data following the method used in seismology. Smaller *b*-value indicates that high amplitude hits are more prevalent. When peak amplitude in decibel is denoted by *A,* and corresponding number of events by *N(A)*, the relation is as follow [10]:

$$\log N(A)=a-b\log(A) \quad (1)$$

where *a* is a constant; *b* is the mentioning *b*-value.

The *b*-values for the C-S-L20-30 concrete are plotted in Fig. 10. Shiotani claimed that the number of AE events to calculate one *b*-value should be 50 or higher [11]. In this experiment, due to the scatter of the data, 200 events were taken. In order to obtain high resolution for *b*-value graph, the sliding window method with step of 25 events was used. The first *b*-value, for example, was calculated based on events from 1 to 200 and then the second *b*-value would be for range from events 26 to 226, etc.

3.3 Classified amplitude distribution

Here, a simple method was employed to study the degree of microcracking. As peak amplitude of AE wave is associated with the magnitude of fracture in material [12], different peak AE amplitude ranges were plotted separately. For example, Fig. 10 shows peak amplitude classification of the C-S-LS20-30 concrete. All AE hits were classified into three categories I, II

and III. Class I consisted of hits with low amplitude, i.e. from 40dB to 50dB. Those for categories II and III were medium (50dB to 60dB) and high amplitude (60dB to 70dB) respectively. As can be seen in Fig. 10, with the time going, low amplitude hits were detected first, followed by medium and high amplitude hits respectively. From the time AE measurement was started (one and half hours after mixing) until when temperature was started decreasing (8 hours), almost only a small number of low amplitude hits (class I) were registered. As temperature went down and autogenous shrinkage further developed, larger microcracks appeared indicated by the beginning of medium amplitude hits. At the age of around 10 hours, highest amplitude AE events (class III) initiated.

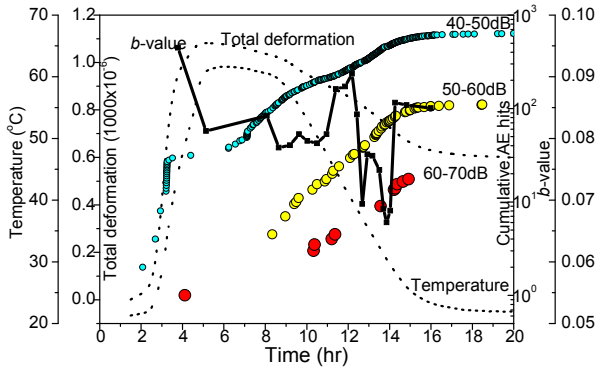

Fig. 10 *b*-value and classified amplitude distribution (C-S-L20-30)

b-value and classified amplitude distribution methods showed good agreement with each other. As can be seen in Fig. 10, *b*-value tended to decrease in the moments when the number of hits increased strongly and when the higher amplitude hits appeared.

However, because *b*-value just presents the relative distribution of peak amplitudes but is not directly connected with the absolute value of the peak amplitude, it may be irrelevant to compare *b*-values obtained from different materials or structures. Dissimilarly, a comparison of quantities of classified AE hits may give a relevant judgement regarding the magnitude of fracture in materials. In Fig. 11a, the cumulative numbers of hits of all three classes detected in C-S-L20-LWA-30 were lower than those of C-S-L20-30. This may imply that lower damage magnitude in concrete with LWA was due to lower potential of localized stress development. When a microcrack occurs, localized stress is released. The potential to build up the same level of local stress to create a new crack by further evolution of net shrinkage of mortar was smaller for concrete with LWA. Also, it may indicate a hint that LWA mortar did not improve cracking resistance significantly but the benefit of using LWA was mainly the lower potential of localized stress induced in material thanks to lower autogenous shrinkage. However, when OPC and GGBFS concretes were compared in Fig. 11b (C-O-L20-30 and C-S-L20-30 respectively), the main differences were for class I and II events. It was possible to suggest that the difference in deterioration in concretes with and without GGBFS was generally attributed to the difference in the number of small microcracks. This information supports the discussion in section 3.1 of this paper that slag concrete tended to crack at lower stress due to lower cracking resistance of slag mortar.

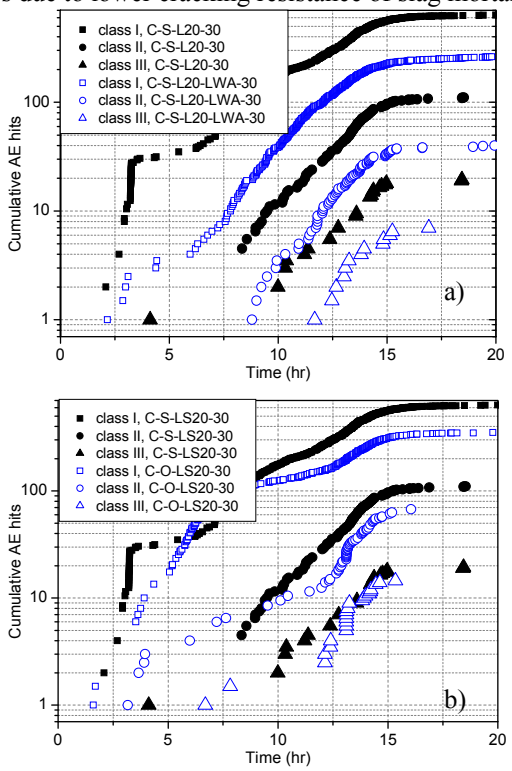

Fig. 11 Classified amplitude distribution, (a) C-S-L20-30 vs C-S-L20-LWA-30 and (b) C-S-L20-30 vs C-O-L20-30

3.4 Microcracking under cyclic temperature

In the previous parts of this paper, the degradation of concrete in the first cycle of variation of temperature has been discussed. The first temperature cycle here was to simulate the condition assumed for the case of heat curing. In this section, further damages in terms of microcracking in concrete caused by cyclic heating-cooling will be studied. When concrete structures are exposed to direct sunlight in the daytimes, the temperature in concrete are expected to vary significantly between daytimes and night times. In these experiments, ten cycles of the same temperature regime were applied for each concrete mix.

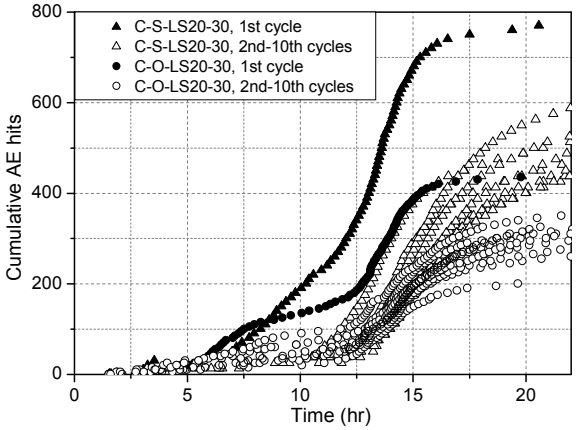

Fig. 12 AE hits in cyclic temperature: C-S-L20-30 and C-O-L20-30

As can be seen in Fig. 12, the numbers of AE hits detected were still significantly high in the later temperature cycles for both GGBFS and OPC concretes. This likely implied that microcracking in the later cycles still occurred considerably. It should be noted that large differences of AE hits detected between the first and the later cycles were partly due to the difference in maximum temperature inside of the specimens. The temperature in the first cycle was about 10^{o}C higher than that in later cycles due to strong cement hydration heat released in the first cycle.

Considering Kaiser effect, the phenomenon found by Kaiser in 1950 [12, 13] where a restart of AE activity only can be observed when the current stress level has reached the maximum experienced stress. In the reloading, concrete behaves elastically until the previous maximum stress level is reached. In this experiment series, concrete specimens were subjected to the same temperature regime in temperature cycles (except the first cycle). Looking at Fig. 12, almost all AE events were detected from the time temperature started to decrease (age of around 8 hours), it was reasonable to take the descending zone of temperature for detail discussion. It is doubtless that the stress in mortar was built up to the maximum level in each cycle when temperature returned to original degree, i.e. around 20^{o}C. These led to a suggestion that if concrete were in a stable condition, there should be no or little AE waves in the later cycles. However, the experimental results showed significant numbers of AE hits even in the later cycles. Hence, this implied that microcracking still took place strongly in the later cycles. The characteristics of AE data of OPC concrete were similar for those of GGBFS but in much lower extent (Fig. 12).

4. CONCLUSIONS

The followings are conclusions obtained from this research.

(1) Extent of microcracking indicated by cumulative AE hits, counts and energy was in rather good agreement with loss of tensile strength of concrete. Damage in concrete with GGBFS was severer than that in concrete with OPC alone.
(2) Microcracking in concrete with GGBFS tended to release lower energy rate, which suggested that microcracking might occur at a lower stress as compared with that in OPC alone concrete.
(3) The benefit of saturated fine LWA was mainly the reduction of potential of localized stress.
(4) The evaluation methods for the degree of microcracking by *b*-value and classified peak amplitude distribution were in good agreement.
(5) Method of classified peak amplitude distribution was simple and comparable between AE data obtained in different concrete materials.
(6) Under mild cyclic temperature, concrete continued to be deteriorated considerably. OPC concrete showed much lower degree of subsequent damage as compared with GGBFS concrete.

ACKNOWLEDGEMENT

This research was funded by Ministry of Education, Culture, Sports, Science and Technology of Japan through the Grant-in-Aid for Young Scientists (B); and the Grant for Construction Technology Development by MLIT.

REFERENCES

[1] Ohtsu, M., "Acoustic emission theory for moment tensor analysis," Research in Nondestructive Evaluation, RILEM, Vol.6, Sep., 1995, pp.169-184
[2] Reginald Hardy, H., "Acoustic Emission – Microseismic Activity," Vol. 1, Principles, Techniques, and Geotechnical Application, A.A. Balkema, 2003, pp.55-58
[3] Son H.N. and Hosoda A., "Mechanical properties of slag cement concrete cured at elevated temperature," 8th International Symposium on Utilization of High-Strength and High-Performance Concrete, 2008, Tokyo, pp.523-528
[4] Bentz, D.P., et al., "Mixture proportioning for internal curing," Concrete International, ACI, Vol.27, Feb., 2005, pp.35-40
[5] Landis, E.N. and Baillon, L., "Experiments to relate acoustic emission energy to fracture energy of concrete," J. of Engineering Mechanics, ASCE, Vol.128, Jun., 2002, pp.698-702
[6] Cusson, D., "Effect of blended cements on effectiveness of internal curing of HPC," Special publication, ACI, Vol.256, Oct., 2008, pp.105-120
[7] Tsiskreli G.D. et al., "The effect of aggregate size on strength and deformation of concrete," Power Technology and Engineering, Vol.4, Jun., 1970, pp.448-453
[8] Elices M. et al., "Effect of aggregate size on the fracture and mechanical properties of a simple concrete," Engineering Fracture Mechanics, Elsevier, Vol.75, Sep., 2008, pp.3839-3851
[9] Landis, E.N., "Acoustic emission in wood," In: Grosse, C. U. and Ohtsu, M., Acoustic emission testing, Springer-Verlag, 2008, pp.311-322
[10] Shiotani, T., et al., "Quantitative evaluation of fracture processes in concrete by the use of improved *b*-value," In: Uomoto T., Non-destructive testing in civil engineering 2000, Elsevier Sicence, 2000, pp.293-302
[11] Shiotani, T., et al., "Application of AE improved *b*-value to quantitative evaluation of fracture process in concrete material." J. of Acoustic Emission, AE Group, Vol.18, 2001, pp.118-133
[12] Shiotani, T., "Parameter analysis." In: Grosse, C. U. and Ohtsu, M., Acoustic emission testing, Springer-Verlag, 2008, pp.41-51
[13] Grosse, C.U., "Sinal-based AE analysis" In: Grosse, C. U. and Ohtsu, M., Acoustic emission testing, Springer-Verlag, 2008, pp.53-100